Heated Supersonic Axisymmetric Jet Cases for the NASA Turbulence Modeling Resource

Nicholas J. Georgiadis[1] and Vance F. Dippold, III[2]
NASA Glenn Research Center, Cleveland, OH 44135

Robert A. Baurle[3]
Air Force Research Laboratory, Wright-Patterson Air Force Base, OH 45433

Christopher L. Rumsey[4]
NASA Langley Research Center, *Hampton, VA 23681*

This paper will describe three new supersonic jet cases for the NASA Turbulence Modeling Resource (TMR). These cases were taken from the 6th AIAA Propulsion Aerodynamics Workshop (PAW) nozzle test problem, which utilized data taken at NASA GRC consisting of non-intrusive measurements of jet plume velocities and temperatures, including both mean values and turbulence statistics. The three jet cases all used a Mach 1.63 axisymmetric nozzle: A heated jet for each at on-design conditions, a temperature-matched on-design condition at Mach 1.63, and an off-design heated condition for the Mach 1.63 nozzle. Computational fluid dynamics (CFD) solutions are obtained using three established Reynolds-averaged Navier-Stokes (RANS) codes: Wind-US, FUN3D, and Vulcan, all using the Menter Shear Stress Transport (SST) k-ω turbulence model. The NASA TMR requires at least two CFD codes yielding essentially identical results to certify that the approaches are verified, that is - providing solutions that may not necessarily provide close comparisons with experimental data, but solve the posed CFD equations as intended.

Nomenclature

a	speed of sound
D	nozzle exit diameter
k	turbulent kinetic energy
M	Mach number
M_a	acoustic Mach number
M_c	convective Mach number
M_j	jet Mach number
M_t	turbulent Mach number
NPR	nozzle pressure ratio = nozzle plenum total pressure / ambient static temperature
Pr_t	turbulent Prandtl number
r	radial coordinate
T	mean static temperature
T'	root-mean-square temperature
T_{jet}	jet exit static temperature
T_t	jet stagnation temperature
T_∞	ambient static temperature
u	mean streamwise velocity
U_{jet}	jet exit velocity
$\overline{u'u'}$	streamwise normal turbulent stress
$\overline{u'v'}$	turbulent shear stress
$\overline{v'v'}$	transverse normal turbulent stress
$\overline{w'w'}$	transverse normal turbulent stress
x	axial coordinate

[1] Aerospace Engineer, Inlets and Nozzles Branch, Georgiadis@nasa.gov, AIAA Associate Fellow
[2] Aerospace Engineer, Inlets and Nozzles Branch, Vance.F.Dippold@nasa.gov, AIAA Senior Member
[3] Senior Technologist for Hypersonics, robert.baurle@us.af.mil, AIAA Associate Fellow
[4] Senior Research Scientist, Computational AeroSciences Branch, c.l.rumsey@nasa.gov, AIAA Fellow

y	transverse coordinate
ΔT	difference between jet static temperature and ambient temperature, $T_{jet} - T_\infty$
ω	specific turbulent dissipation rate

Introduction

The NASA Turbulence Modeling Resource[1-2] (TMR) is a website containing detailed information on Reynolds-averaged Navier-Stokes (RANS) turbulence models as well as several test cases intended to benchmark computational fluid dynamics (CFD) codes against experimental data and expected solutions using certified computational solutions. Naturally, the first test cases constructed were canonical cases having relatively simple geometry flows at relatively low subsonic speeds. Over time, flow cases with varying aerodynamic challenges have been added. These cases include wall bounded flows at a range of Mach numbers up to supersonic speeds and free shear layer flows, including three jet subsonic jet cases. These subsonic jet cases all utilized convergent nozzles with jet plume measurements taken by Bridges and Wernet[3-4] Two supersonic cases, measured against heated supersonic jet data of Seiner et. al[5], are also available. The experimental data available for these supersonic jet cases consists of centerline velocities and temperatures, measured with traditional stagnation temperature and pressure probes. The TMR cases for these Mach 2 jets have comparisons of CFD to experiment for calculations obtained with the Spalart-Allmaras model.[6] Numerous computational efforts have utilized this set of experimental data to evaluate Reynolds-averaged Navier-Stokes (RANS) CFD methods, with Refs. 7–12 as only a few examples. Several other efforts[13-17] have used the data to propose modifications to RANS methods for calculation of heated supersonic jets. Morris and Luke[18] modeled these experiments with implicit large eddy simulation (LES).

More recently, experimental data collected at NASA Glenn Research Center, Refs. 19-21, built upon the earlier Seiner experiments to use non-intrusive measurements of both velocities and temperatures for a series of supersonic jets. These newer experiments included Mach 2 jet cases to benchmark results against the earlier efforts of Seiner et. al, and established close agreement with the former data collected using centerline total temperature and total pressure probe measurements. The newer data was used in the 6th Propulsion Aerodynamics Workshop (PAW) sponsored by the American Institute of Aeronautics and Astronautics (AIAA) to investigate both RANS techniques as well as scale-resolving simulation (SRS) approaches. SRS employ large eddy simulation in the focus region of a flow problem which for supersonic jets is the jet plume mixing region. Results using RANS and SRS approaches obtained in the 6th PAW for the newer NASA GRC experiments are provided in Georgiadis et al.[22]

Supersonic jet flow fields have been studied extensively over the years, with interest in understanding and predicting jet plume mixing for purposes of acoustics, plume thermal impacts, and mixing characteristics. While round jets are relatively simple geometrically, the flow physics of heated supersonic jets have remained challenging for computational fluid dynamics (CFD) methods to model accurately. The primary difficulties are accurately replicating the effects of turbulent thermal transport and reduced mixing rate due to compressibility. The objective of the 6th PAW nozzle test case was to assess the accuracy of existing CFD codes and modeling techniques in simulating the aerodynamics and thermodynamics of heated supersonic jet plumes from axisymmetric convergent-divergent (C-D) nozzles. Previous workshops focused on nozzle aerodynamics, propulsion efficiency, and heat transfer metrics. This paper uses 3 of the cases utilized during the workshop to construct new axisymmetric jet cases for the NASA TMR.

Nozzle/Jet Case Details

A. Nozzle Experimental Configuration:

In the PAW, 3 axisymmetric convergent-divergent nozzles, designed using the method of characteristics to provide as close to a uniform nozzle exit flow free of shock waves as possible, were investigated. The nozzles were designed to provide Mach 1.36, 1.63, and 2.00 perfectly expanded flows at the nozzle exit. For the TMR cases discussed here, only the Mach 1.63 nozzle was used, with three operating points selected as shown in Table 1. The case number shown in the first column table refers to the case number designation from the PAW workshop.

In the experiments, the nozzle was operated by controlling the supply total pressure to achieve the jet exit Mach number (M_{jet}) corresponding to a given nozzle pressure ratio (NPR = supply total pressure divided by ambient static pressure) and nozzle static temperature difference (ΔT = calculated jet exit static temperature - ambient static temperature). It is standard in many aerodynamic CFD simulations to assume a calorically perfect gas, such that the specific heat ratio, γ, is constant, and if the working fluid is air, $\gamma = 1.4$. The NPR and calculated jet Mach number, M_{jet}, shown in Table 1 assumes $\gamma = 1.4$. For the calculations to be obtained for these cases, this is an acceptable assumption, and employing a variable γ capability was not expected to change the results significantly. In the

experiments, hydrogen was combusted to heat the air to the desired temperature. The primary effects of H_2O in the exhaust gas are to slightly reduce the nozzle flow rate and to minimally change the gas properties.

Table 1. Operating Conditions

PAW6 Case	Nozzle Geometry Mach No.	Nozzle Operating Mach No.	NPR	Nozzle Tt (K)	Jet ΔT (K) = $T_{jet} - T_\infty$	U_{jet} (m/s)	M_c	M_a
5	1.63	1.63	4.44	442.1	0	555.2	0.68	1.36
2	1.63	1.63	4.44	799.4	233	746.6	0.93	2.19
4	1.63	1.36	3.01	715.2	233	594.0*	0.78	1.83

**U_{jet} based on supply conditions would be the same as for case 1 (622.9 m/s) but as discussed in the Results section, a normal shock reduces the effective U_{jet} to 594.0.*

The convective Mach number (M_c) shown in Table 1, as defined in Eqn. 1, is a measure of the compressibility of the jet. The acoustic Mach number (M_a), as defined in Eqn. 2, is used in the jet aeroacoustics community to relate the jet exhaust speed to the ambient air speed of sound and hence characterize the propagation of jet mixing noise. Bridges and Wernet[3-4] employed M_a to assemble the matrix of convergent nozzle jets in their experiments. A nearly sonic heated jet can have $M_j < 1$ but $M_a > 1$. Also note that for a temperature matched jet, such as Case 5 in Table 1 where $T_{jet} = T_\infty$, $M_a = 2\ M_c$.

$$M_c = u_{jet} / (\sqrt{\gamma R T_{jet}} + \sqrt{\gamma R T_\infty}) \quad (1)$$

$$M_a = u_{jet} / \sqrt{\gamma R T_\infty} \quad (2)$$

During the tests, the freestream conditions varied from day-to-day and even during a single day's testing, but for the purposes of CFD investigations, Ref. 22 recommend using a constant assumed static pressure of 99.28 kPA (14.4 psi) and static temperature of 288.9 K (520 R) for the ambient conditions. These were reference ambient properties used to calculate the ideal jet exit velocities shown in Table 1.

The first case in the table (PAW Case 5) is for the Mach 1.63 nozzle, with on-design pressure ratio and has ΔT = 0 K, or in other words, no static temperature difference between the nozzle exhaust and the ambient air at the nozzle exit. The second case (PAW Case 2) shown in Table 1 represents on an-design Mach 1.63 nozzle flow with jet exit ΔT = 233 K. The last case in the table (PAW Case 4) examines an off-design, overexpanded case where the Mach 1.63 nozzle is run at flow supply conditions identical to that of the first case, which is on-design for the Mach 1.36 nozzle. In other words, the NPR of this fourth case is too low to result in a fully expanded state at the nozzle exit for the Mach 1.63. For the NASA TMR, these three jet cases will be referred to as **"Temperature-Matched Mach 1.63 Axisymmetric Jet," "Heated Mach 1.63 Axisymmetric Jet,"** and **"Off-Design Mach 1.63 Axisymmetric Jet,"** respectively.

B. Computational Grids:

A set of computational grids were developed for the PAW and used here for the TMR cases with a RANS structured topology using the Pointwise[23] software to create meshes for the axisymmetric geometry, with the axis of the nozzle and jet serving as the bottom of the grid. A view of the computational grid constructed for the Mach 1.63 nozzle is shown in Fig. 1. The internal geometry of the experimental test article is reproduced as far upstream as the supply pipe. The geometry of the outside of the nozzle, adapter, and supply pipe, is also modeled very closely with the exception that in this axisymmetric representation, the regions of the external surface locations where fasteners were used to attach the components of the assembly were faired over. As the nozzle experiments were run with zero co-flow, this change is not expected to be a significant modeling deviation. At the exit plane of the nozzle the lip thickness is 0.5 mm.

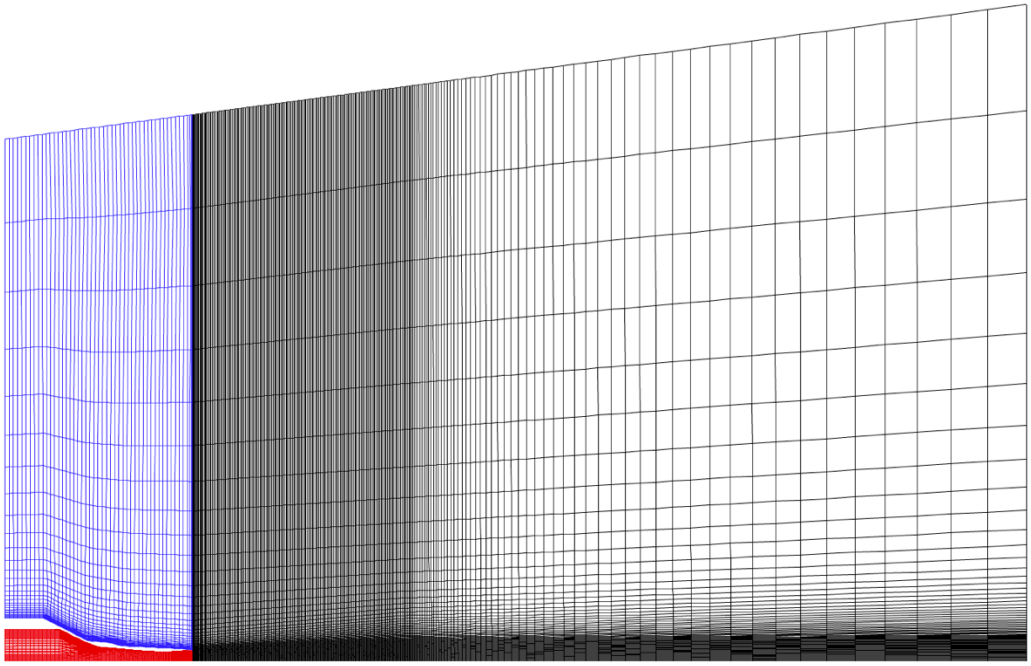

(a) Entire grid

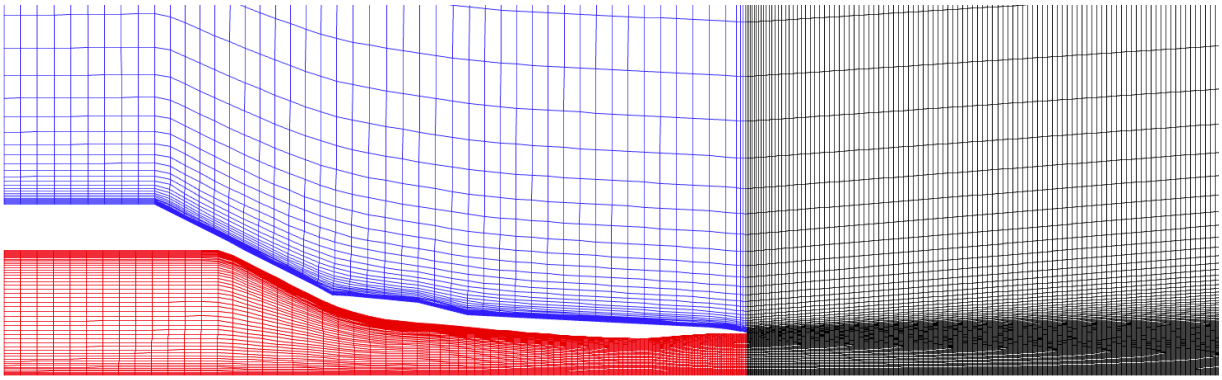

(b) detail near nozzle exit

Figure 1.—Computational grid for Mach 1.63 nozzle (every 4th point shown in the axial and radial directions for clarity).

Using the structured grid approach, three zones were utilized with point-to-point matching at zonal interfaces. The location of the axis of symmetry at the nozzle exit is set as the origin of the computational domain (i.e. x,r = 0,0). Three zones comprised of: (1) nozzle internal region (401 axial points by 281 radial points), (2) external nozzle region and extending radially (201 by 161 points), (3) the jet plume region (961 by 481 points). All of these grid counts are for the finest level. The nozzle lip has 41 points. The axial spacing of the grid at the nozzle exit was 0.005D, and the grids extended 40D to the outflow boundary. Radially, the second zone has an inflow plane that extends 25D away from the centerline. The farfield boundary has a 7.5 degree divergence angle, starting from zone 2 and extending into zone 3, to ensure that any entrained ambient air enters the flow domain. As a result, at the jet plume zone outflow station (at x/D = 40) in zone 3, the farfield boundary extends to 32.45D.

The supplied structured grids may be coarsened to study RANS solver grid convergence following the philosophy of cases available on the NASA Turbulence Modeling Resource[1-2]. These grids may be sequenced (i.e. agglomerated by removing every other point) in each direction 3 times to provide 4 grid sets with: (1) un-sequenced: 401 × 281,

201 × 161, 961 × 481, (2) 1-level sequenced: 201 × 141, 101 × 81, 481 × 241, (3) 2-level sequenced: 101 × 71, 51 × 41, 241 × 121, (4) 3-level sequenced: 51 × 36, 26 × 21, 121 × 61.

The grid was packed such that the nominal y+ of the first point off the wall in the supersonic portion of the nozzle was on the order of 1. With only entrained slow flow outside the nozzle, the wall spacing on the external portion of the nozzle was packed much less tightly. Zones 2 and 3 are identical for the grids with each of the 3 C-D nozzles.

Note, these computational grids were built and checkout runs were conducted using CFD strategies very similar to the three test cases available via the NASA turbulence modeling resource (turbmodels.larc.nasa.gov), namely the "Axisymmetric Subsonic Jet," "Axisymmetric Hot Subsonic Jet," and "Axisymmetric Near-sonic Jet" cases. The three-zone approach and overall gridding strategies were similar to the grids discussed here for the supersonic jet cases, although finer grid resolution in the potential core region was used here for the supersonic cases, especially needed for the off-design case with shock waves in the jet plume.

D. Boundary Conditions and Flow Solver Settings:

The boundary conditions required to run these nozzle cases are relatively straightforward, at least for a steady RANS approach. The stagnation pressure and temperature for each case may be obtained from Table 1 and applied at the inflow to the nozzle. In the experiments, there was no co-flow, but some forward velocity needs to be prescribed with most CFD solvers to enable convergence. Preliminary test calculations were performed for the grids discussed in the previous section with multiple flow solvers utilizing a freestream condition set to Mach 0.01. It is generally desirable to set this freestream Mach number as low as possible but increasing it as high as Mach 0.05 did not affect the jet solutions significantly in this case. On the finest grid level, many general purpose RANS solvers have difficulty obtaining converged steady-state solutions with a constant CFL solver approach. Completing these solutions with a time-accurate (constant time step) approach is frequently required to obtain a thoroughly converged RANS solution. As suggested previously, a constant assumed static pressure of 99.28 kPA (14.4 psi) and static temperature of 288.9 K (520 R) was used for the ambient conditions in these simulation cases.

It is believed that the flows inside the nozzles generated turbulent boundary layers, although measurements were not made inside the nozzle to verify this. Heat transfer to the nozzle structure was not expected to be a significant factor, so adiabatic wall boundary conditions could be set for the interior and exterior surfaces of the nozzle. The nozzle structure was constructed from 316 stainless steel which does not have a high thermal conductivity. The default turbulent Prandtl number (Pr_t) used in most production CFD codes is 0.9 but there are some studies[24] which have indicated that using $Pr_t = 0.7$ maybe more accurate for jet flows.

Approaches Utilized by Workshop Participants

Three widely used RANS-based solvers were used for the preliminary investigations discussed in this paper: Wind-US,[25] FUN3D[26], and Vulcan[27]. For the baseline results shown in this paper, all codes employed the Shear Stress Transport (SST) k-ω model of Menter[28-29] using vorticity production term for the turbulent kinetic energy. On the NASA TMR, this form of the model is referred to as SST-Vm. After these cases are established on the TMR website, it is expected that additional turbulence models will be added, but the results here utilize the SST-V two-equation model because it is one of the most widely used RANS models for jet flows. Wind-US and Vulcan utilized structured flow solvers and FUN3D utilized an unstructured flow solver, and all used the workshop provided structured meshes.

Results

A. Temperature-Matched Mach 1.63 Axisymmetric Jet:

The temperature matched case was set experimentally by heating the nozzle plenum flow to a total temperature that when expanded through the convergent divergent nozzle to a Mach 1.63 exit state, yielded a static temperature that matched that of the ambient, and hence provided no mean thermal gradient. A comparison of computational solutions obtained with the three CFD codes is made with experimental data for centerline velocities and turbulent kinetic energy in Figs. 2-3. As expected, the RANS predictions overpredict mixing rate for these supersonic jets. Compressibility effects, which slow the experimentally measured mixing relative to incompressible jets, are not captured accurately by uncorrected two-equation turbulence models. Recall, however, the purpose of these TMR cases is not detailed scrutiny of the performance of the RANS modeling, but rather establishing the expected benchmark results for a given RANS turbulence model.

The mean velocities shown in Fig. 2 and turbulent kinetic energy results shown in Fig. 3 demonstrate that all of the solutions predict higher centerline turbulent kinetic energy levels than those measured experimentally. The

experimental streamwise PIV data used to compare to the computational results did not measure $\overline{w'w'}$, but Ref. 19 showed that it can be reasonably approximated as $\frac{3}{2}\overline{v'v'}$, and k can be approximated as shown in Eqn. 3.

$$k = \frac{1}{2}(\overline{u'u'} + \overline{v'v'} + \overline{w'w'}) \approx \frac{1}{2}\left(\overline{u'u'} + \overline{v'v'} + \frac{3}{2}\overline{v'v'}\right) = \frac{1}{2}\overline{u'u'} + \frac{5}{4}\overline{v'v'} \quad (3)$$

All of the RANS solutions exhibit essentially no centerline turbulent kinetic energy until an axial location corresponding to the end of the potential core. Then there is an abrupt rise in turbulent kinetic energy levels near x/D = 8. In contrast, the experimental data exhibits a more gradual initial increase in turbulent kinetic energy levels that initiates before the end of the potential core, around x/D = 5. The actual jet has a potential core length that instantaneously varies in time and as a result there is intermittent turbulence. This upstream turbulence arises from the portion of time when the jet potential core is shorter than the mean potential core length. The RANS solutions, which by design are only representing a time averaged solution, are generally unable to replicate this intermittent turbulence appearing before the end of the mean jet potential core, starting at about x/D = 5.

Profiles of axial velocity, turbulent kinetic energy, and turbulent shear stress are provided in Fig. 4 at several axial stations in the jet plume. Close agreement is observed between the three codes for all quantities, although the discrepancy of the solutions with experimental data is readily apparent. The close agreement of the three flow solvers establishes that the same modeling approach in independent flow solvers, should be expected to yield similar results of jet flow predictions.

B. Temperature-Matched Mach 1.63 Axisymmetric Jet:

The comparison of centerline velocities and turbulent kinetic energy for the heated case, shown in Figs. 5-6, show similar agreement to that for the unheated case in the previous section. However, when using the default output from the three RANS codes for temperatures (Fig. 7), it was noted that the Vulcan result was substantially different than that from the other two codes. It was found that the form of the total energy equation solved by Vulcan differed from that of Wind-US and FUN3D, in that Vulcan included the turbulent kinetic energy while the other two codes ignored this contribution to the total energy. For lower speed flows without significant thermal effects, this is usually an acceptable assumption and does not have a significant effect on aerodynamic predictions. However, ignoring this term in compressible heated flows can have an appreciable effect as is demonstrated here. As a post-processing step, adding the turbulent kinetic energy to compute equivalent temperature for Vulcan as if it likewise ignored this contribution to total energy, resulted in values for centerline temperature that are very close to that provided by the other two codes.

Profiles of axial velocity, turbulent kinetic energy, and turbulent shear stress are provided in Fig. 8 at several axial stations in the jet plume. Again, the velocity and turbulent statistics shown here are unaffected by the assumption of whether or not to include the turbulent kinetic energy in the total energy equation. However, the static temperature profiles are affected by the treatment of the total kinetic energy (Fig. 9). Only the default Vulcan solution, that subtracts the turbulent kinetic energy before computing internal energy and hence static temperature, is shown on these profiles. When ignoring the turbulent kinetic energy, Vulcan and the other two codes yield nearly identical static temperature profiles.

C. Off-Design Mach 1.63 Axisymmetric Jet:

A comparison of centerline velocities for the off-design case is shown in Fig. 10. More details for this case will be shown in the final paper, in parallel to the results showed for the other two test cases.

Conclusions and Work for Final Paper

This extended abstract provides preliminary comparisons of three RANS solvers for three new supersonic heated jet cases for the NASA Turbulence Modeling Resource (TMR). Preliminary results show very close agreement of the three codes when using similar assumptions and the same turbulence model. The heated jet case is essentially the first from the TMR to directly compare to in-flow measured temperatures. Through comparison with this temperature data, it was found that the default treatment for turbulent kinetic energy in the total energy equation solved by these three codes differed and resulted in noticeable differences in predicted jet temperatures.

In the final paper, more details for the off-design case will be presented. In addition, grid sensitivity effects will be discussed. While not presented in this extended abstract, it was found that the dense axisymmetric grids employed here yielded virtually identical solutions on sequenced coarser grids.

Acknowledgments

This work was supported by the Transformational Tools and Technologies (TTT) Project of NASA's Transformative Aeronautics Concepts Program (TACP) and Hypersonic Technology Project (HTP) of the Advanced Air Vehicle Program (AAVP).

References

1. Rumsey, C., Smith, B., and Huang, G., "Description of a Website Resource for Turbulence Modeling Verification and Validation," AIAA Paper 2010-4742, June 2010.
2. Rumsey, C. L., "Recent Developments on the Turbulence Modeling Resource Website (Invited)," AIAA Paper 2015-2927, June 2015.
3. Bridges, J. and Wernet, M. P., "Establishing Consensus Turbulence Statistics for Hot Subsonic Jets," AIAA Paper 2010-3751, June 2010.
4. Bridges, J. and Wernet, M. P., "The NASA Subsonic Jet Particle Image Velocimetry (PIV) Dataset," NASA-TM 2011-216807, Nov. 2011.
5. Seiner, J. M., Ponton, M. K., Jansen, B. J., and Lagen, N. T., "The Effect of Temperature on Jet Noise Emission," AIAA Paper 92-02-046, 1992.
6. Spalart, P. R. and Allmaras, S. R., "A One-Equation Turbulence Model for Aerodynamic Flows," *La **Recherche Aerospatiale**,* Vol. 1, 1994, pp. 5-21.
7. Abdol-Hamid, K. S., Carlson, J. R., and Rumsey, C. L., "Verification and Validation of the k-kL Turbulence Model in FUN3D and CFL3D," AIAA Paper 2016–3941, Jan. 2016.
8. Yoder, D. A., Georgiadis, N. J., and O'Gara, M. R., "Frozen Chemistry Effects on Nozzle Performance Simulations," AIAA Paper 2008-3969, Jan. 2008.
9. Dembowski, M. A. and Georgiadis, N. J., "An Evaluation of Parameters Influencing Jet Mixing Using the WIND Navier-Stokes Code," NASA TM 2002-211727, Aug. 2002.
10. Barber, T. J., Chiapetta, L. M., DeBonis, J. R., Georgiadis, N. J., and Yoder, D. A., "Assessment of Parameters Influencing the Prediction of Shear Layer Mixing," ***Journal of Propulsion and Power***, Vol. 15, No. 1, 1998, pp. 45–53.
11. Abdol-Hamid, K. S., Carlson, J. R., and Rumsey, C. L., "Verification and Validation of the k-kL Turbulence Model in FUN3D and CFL3D," AIAA Paper 2016–3941, Jan. 2016.
12. Georgiadis, N.J., Yoder, D.A., Vyas, M.A., and Engblom, W.A., "Status of Turbulence Modeling for Hypersonic Propulsion Flowpaths," ***Theor. Comput. Fluid Dyn***., Vol. 28, 2014, pp. 295-318.
13. Papp, J. and Dash, S., "Turbulence Model Unification and Assessment for High-Speed Aeropropulsive Flows," AIAA Paper 2001–0880, Jan. 2001.
14. Papp, J., Kenzakowski, D., and Dash, S., "Calibration and Validation of EASM Turbulence Model Jet Flowfields," AIAA Paper 2002–0855, Jan. 2002.
15. Tam, C. K. W. and Thies, A. T., "Computation of Turbulent Axisymmetric and Nonaxisymmetric Jet Flows Using the k-ϵ Model," ***AIAA Journal***, Vol. 34, No. 2, Feb. 1996, pp. 309–316.
16. Tam, C. K. W. and Ganesan, A., "A Modified k-ε Turbulence Model for Calculating the Hot Jet Mean Flows and Noise," ***AIAA Journal***, Vol. 42, No. 1, Jan. 2004, pp. 26–34.
17. Abdol-Hamid, K. S., Pao, S. P., Massey, S. J., and Elmiligui, A., "Temperature Corrected Turbulence Model for High Temperature Jet Flow," ***Journal of Fluids Engineering***, Vol. 126, No. 5, 2004, pp. 844–850.
18. Morris, C. I. and Luke, E. A., "Implicit Large-Eddy Simulations of Hot and Cold Supersonic Jets in Loci-CHEM," AIAA Paper 2020-1333, Jan. 2020.
19. Georgiadis, N. J., Wernet, M. P., Locke, R. J., and Eck, D. G., "Mach Number and Heating Effects on Turbulent Supersonic Jets," ***AIAA Journal***, Vol. 62, No. 1, Jan. 2024.
20. Wernet, M. P., Georgiadis, N. J., and Locke, R. J., "Raman Temperature and Density Measurements in Supersonic Jets," ***Experiments. In Fluids***, Vol. 62, No. 3, 2021, pp. 1-21.
21. Wernet, M. P., Georgiadis, N. J., and Locke, R. J., "Velocity, Temperature and Density Measurements in Supersonic Jets," NASA/TM-20205007269 and AIAA Paper 2021-0596, Oct. 2020.
22. Georgiadis, N. J., Wernet, M. P., Winkler, C.M., Benton, S.I., and Connolly, B.J., "Summary of the 6th Propulsion Aerodynamics Workshop Nozzle Test Case: Heated Supersonic Axisymmetric Jets," AIAA Paper 2024-0749, Jan. 2024.
23. Pointwise, Version 18.3 Release 1 [Software]. 2021. URL: https://www.pointwise.com/
24. Birch, S. F., Lyubimov, D. A., Maslov, V. P., Secundov, A. N., and Yakubovsky, K. Y., "A RANS Based Jet Noise Prediction Procedure," AIAA Paper 2007-3727, June 2007.
25. Yoder, D.A., "Wind-US User's Guide," NASA TM2016-210145, Sept. 2016.
26. Biedron, R. T., Carlson, J. R., Derlaga, J. M., Gnoffo, P. A., Hammond, D. P., Jones, W. T., Kleb, B., Lee-Rausch, E. M., Nielsen, E. J., Park, M. A., Rumsey, C. L., Thomas, J.L., and Wood, W. A., "FUN3D User's Manual Version 13.3," NASA/TM 2018-219808, Feb. 2018.
27. Baurle, R. A., White, J.A ., Drozda, T. G., and Norris, A. T., "Vulcan-CFD Theory Manual: Ver. 7.2.0,: NASA TM 2022-000-8776, Nov. 22.
28. Menter, F. R., "Improved Two Equation k-ω Turbulence Models for Aerodynamic Flows," NASA/TM 103975, Oct. 1992.

29. Menter, F. R., "Two Equation Eddy-Viscosity Turbulence Models for Engineering Applications," ***AIAA Journal***, Vol. 32, No. 8, 1994, pp. 1598-1605.

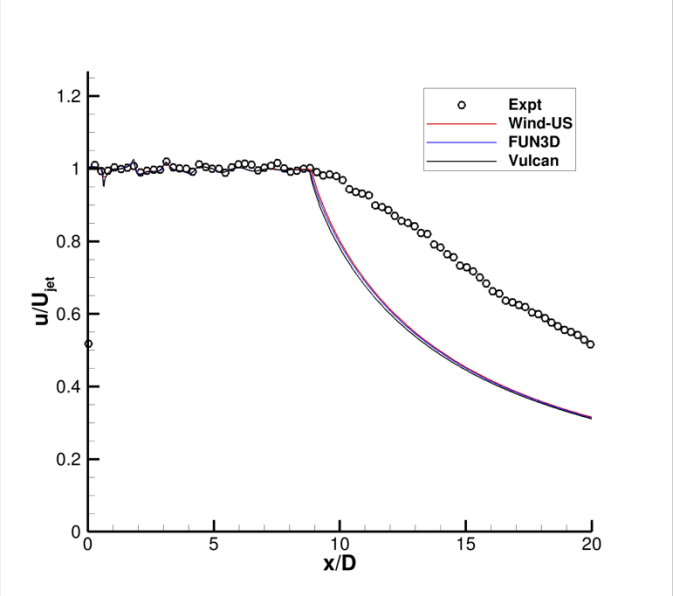

Figure 2.— Centerline velocity comparisons for the temperature matched case.

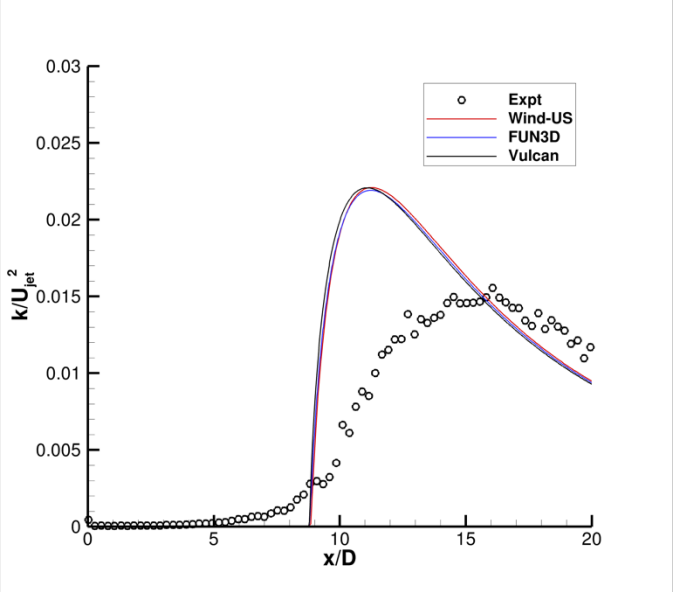

Figure 3.— Centerline turbulent kinetic energy comparisons for the temperature matched case.

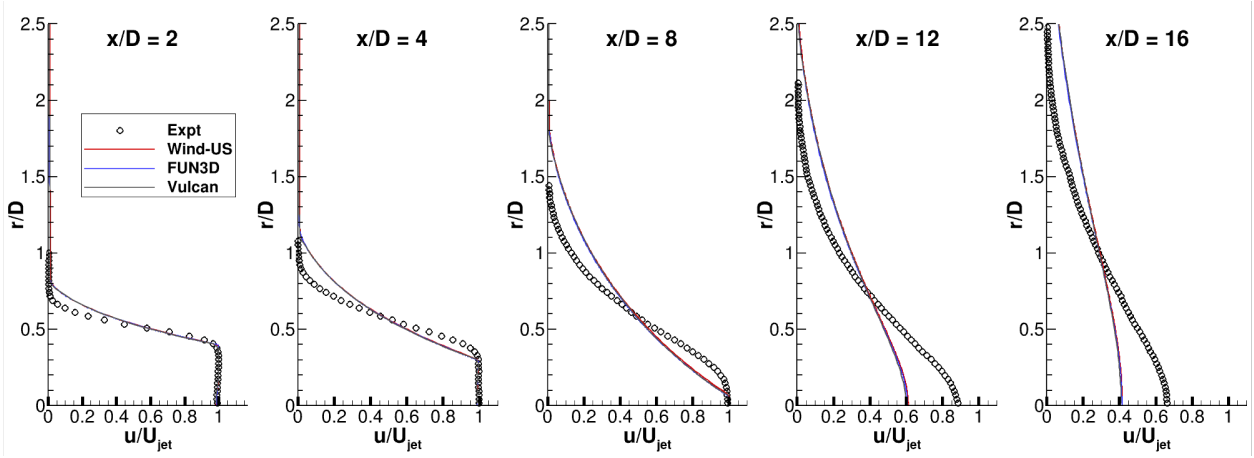

(a) Axial velocity

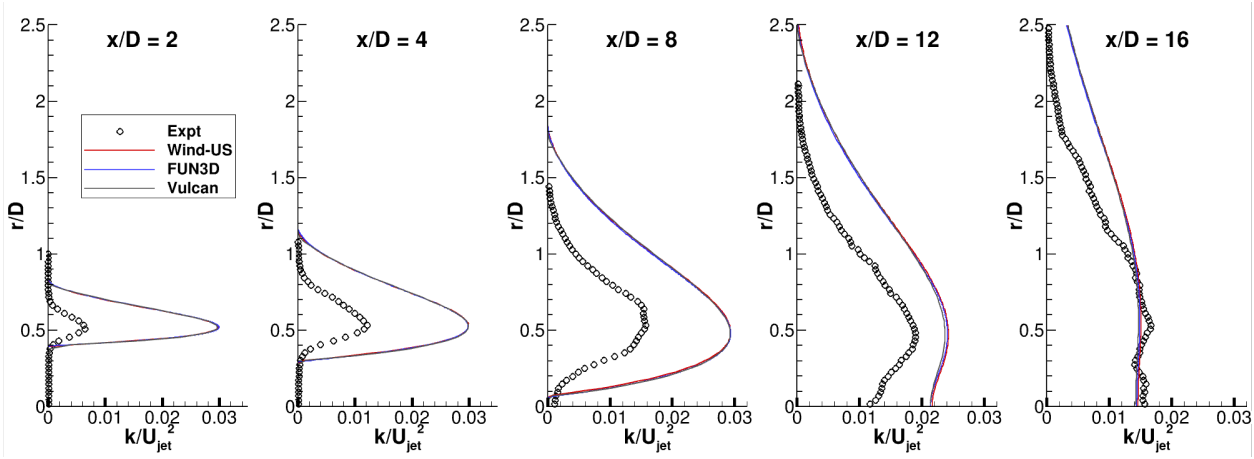

(a) Turbulent kinetic energy

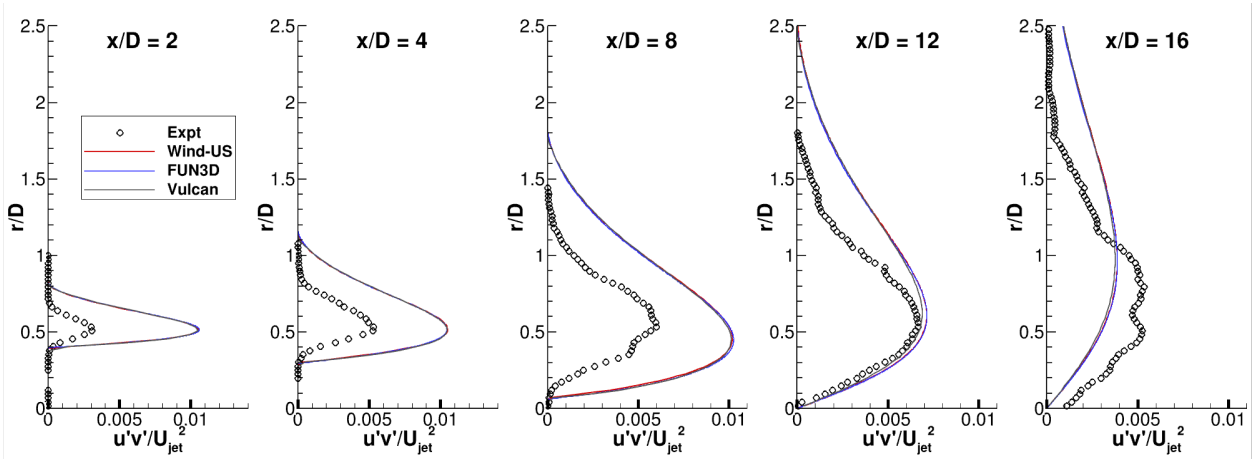

(b) Turbulent shear stress

Fig. 4 Axial profiles of flow quantities for the temperature matched case.

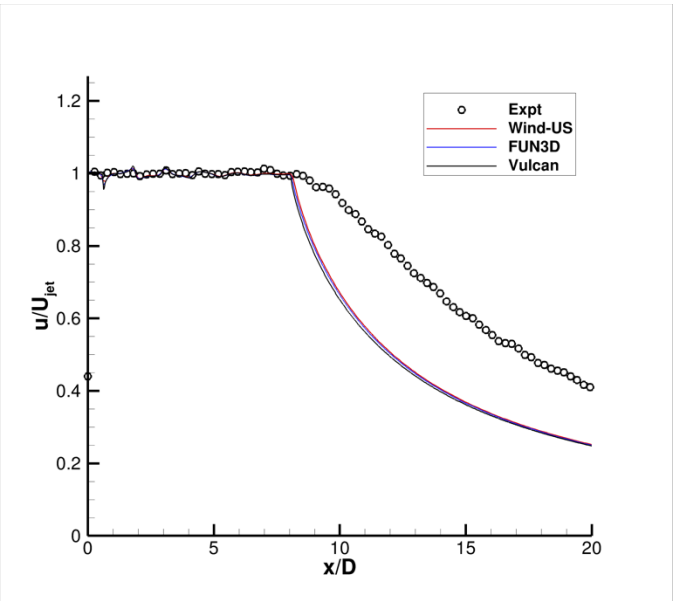

Figure 5.— Centerline velocity comparisons for the heated Mach 1.63 jet case.

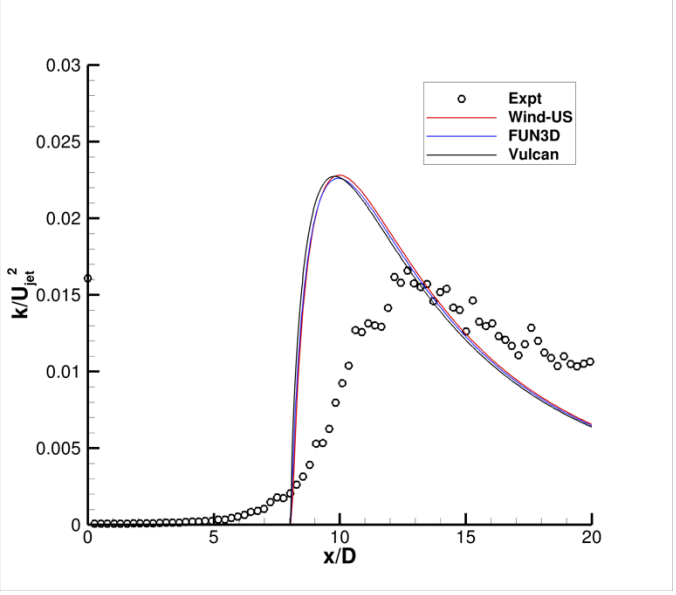

Figure 6.— Centerline turbulent kinetic energy comparisons for the heated Mach 1.63 jet case.

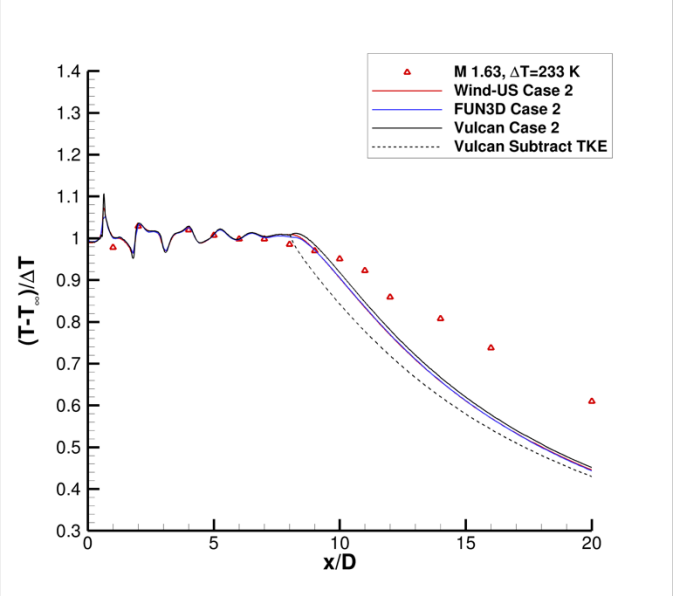

Figure 7.— Centerline temperature comparisons for the heated Mach 1.63 jet case.

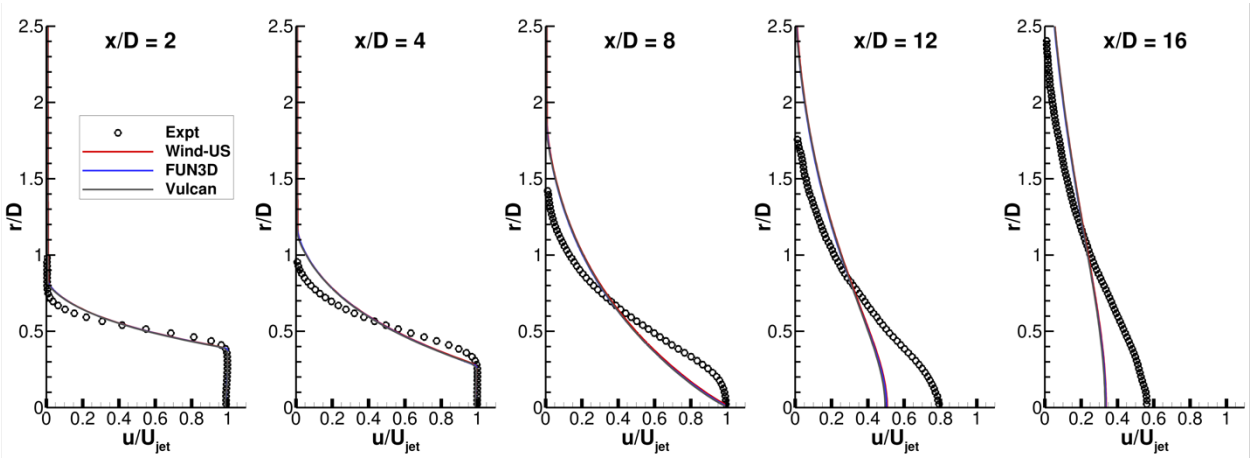

(a) axial velocity

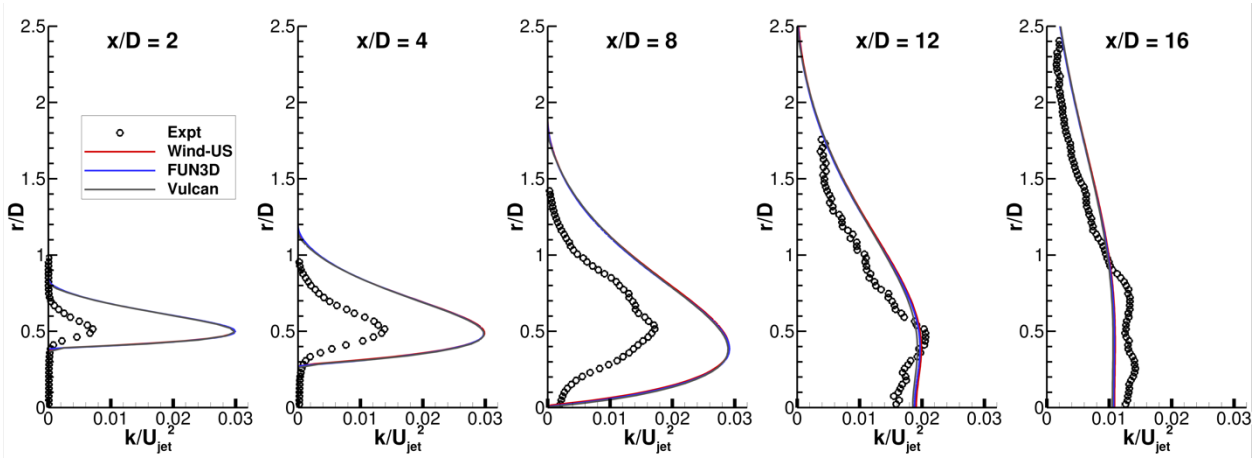

(b) Turbulent kinetic energy

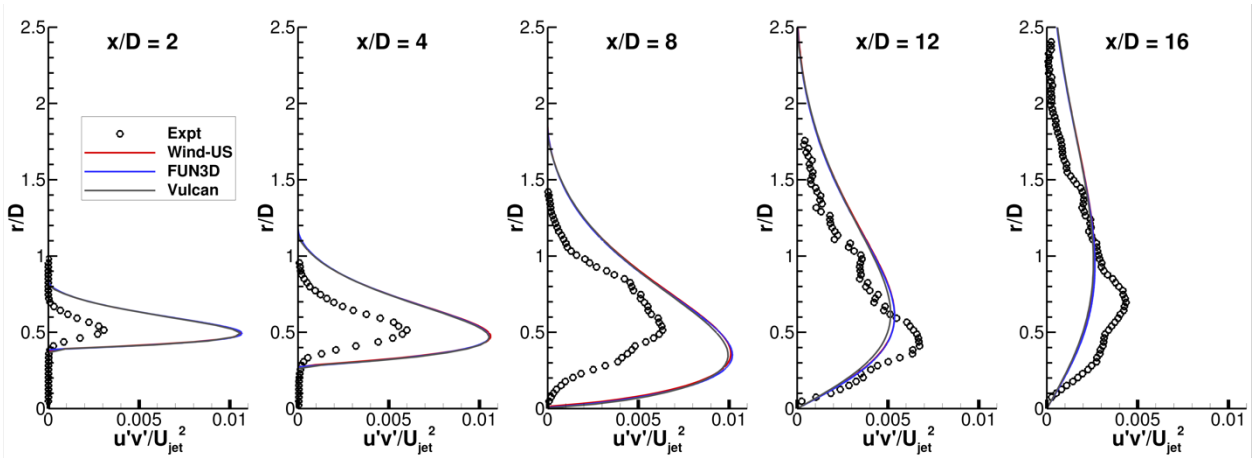

(c) turbulent shear stress

Fig. 8. Axial profiles of flow quantities for the heated jet case.

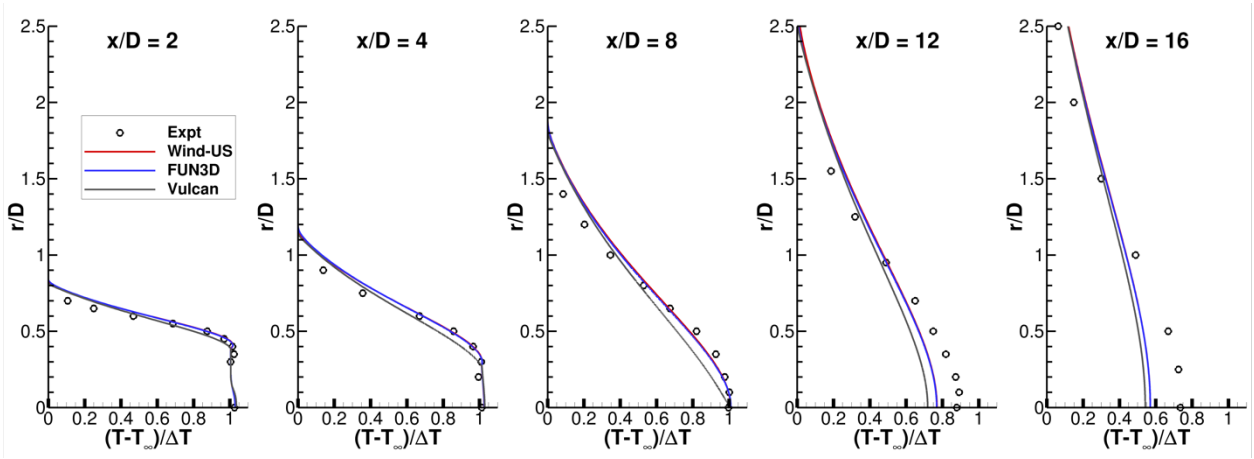

Figure 9.— Static temperature comparisons for the heated jet case.

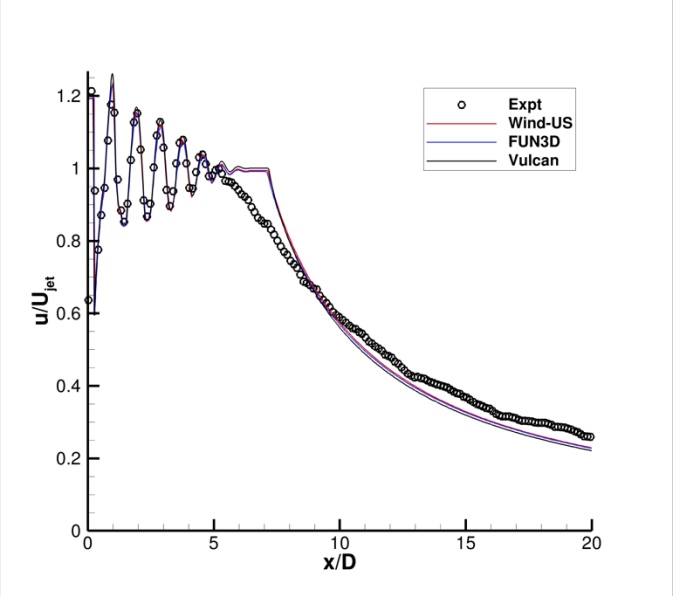

Figure 10.— Centerline velocity comparisons for the off-design jet case.